crystals

MDPI

Article

Triarylazoimidazole-Zn^{II}, Cd^{II}, and Hg^{II} Complexes: Structures, Photophysics, and Antibacterial Properties

Alexey A. Artemjev [1], **Artyom A. Astafiev** [2], **Anna V. Vologzhanina** [3], **Alexey S. Kubasov** [4], **Gleb M. Burkin** [1], **Alexander S. Novikov** [5], **Andreii S. Kritchenkov** [1], **Anatoly A. Kirichuk** [1] and **Alexander G. Tskhovrebov** [1,2,*]

1   Research Institute of Chemistry, Peoples' Friendship University of Russia, Miklukho-Maklaya Str. 6, 117198 Moscow, Russia; artemyev-ala@rudn.ru (A.A.A.); burkin-gm@rudn.ru (G.M.B.); platinist@mail.ru (A.S.K.); kirichuk-aa@rudn.ru (A.A.K.)
2   N.N. Semenov Federal Research Center for Chemical Physics, Russian Academy of Sciences, Kosygina 4, 119991 Moscow, Russia; astafiev.artyom@gmail.com
3   A.N. Nesmeyanov Institute of Organoelement Compounds, Russian Academy of Sciences, Vavilova Str. 28, 119334 Moscow, Russia; vologzhanina@mail.ru
4   N.S. Kurnakov Institute of General and Inorganic Chemistry, Russian Academy of Sciences, Leninsky Prt. 31, 119071 Moscow, Russia; fobosax@mail.ru
5   Institute of Chemistry Saint Petersburg State University, Universitetskaya Nab. 7/9, 199034 Saint Petersburg, Russia; a.s.novikov@spbu.ru
*   Correspondence: tskhovrebov-ag@rudn.ru

Abstract: Novel triarylazoimidazoles containing strong electron donors (*p*-NEt$_2$) or acceptors (*p*-NO$_2$) by the azoaryl group, and their group 12 metal complexes were synthesized and fully characterized, including X-ray analysis for several complexes. Novel complexes exhibit red photo-luminescence emission (Φ up to 0.21) in a solution. Moreover, the antibacterial activity of complexes was tested against Gram-positive microorganism *S. aureus* and Gram-negative microorganism *E. coli*.

1. Introduction

Imidazole function is an important group in biology, often playing a role as a supporting ligand in metal-containing systems [1–3]. This stimulates the synthesis and structural characterization of imidazole metal complexes to better understand the role of these ligands. Azoimidazoles constitute an important class of photoactive materials, which were intensively studied earlier [4–9]. In addition, they are interesting chelating ligands, which electronics could be easily modulated via facile structural tuning [6,8,10]. Recently we started exploring triarylazoimidazoles and their coordination compounds [2,11,12]. Surprisingly, triarylazoimidazoles received almost no attention in the literature. In our recent publication, we showed that coordination of some triarylazoimidazoles to Zn^{II}, Cd^{II}, and Hg^{II} led to the formation of bright red emissive complexes (quantum yields up to 44%), which could be excited with a visible light [2]. Here, we report the synthesis and structural characterization of several novel triarylazoimidazoles and their emissive group 12 metal complexes (Φ up to 0.21). Introduction of the *p*-bromo substituent to the azoaryl substituent of the Zn-coordinated triarylazoimidazole shifts an emission maximum to 677 nm relatively to the unsubstituted triarylazoimidazole complex. In addition, we report antibacterial properties of novel complexes.

2. Materials and Methods

General remarks. Unless stated otherwise, all the reagents used in this study were obtained from the commercial sources (Aldrich (Schnelldorf, Germany), TCI-Europe (Zwi-

jndrecht, Belgium), Strem (Bischheim, France), and ABCR (Karlsruhe, Germany)). NMR spectra were recorded on a Bruker Avance III (Karlsruhe, Germany) (^{1}H: 400 MHz); chemical shifts (δ) are given in ppm relative to TMS, coupling constants (J) in Hz. The solvent signals were used as references (CDCl$_3$: δ_C = 77.16 ppm; residual CHCl$_3$ in CDCl$_3$: δ_H = 7.26 ppm; CD$_2$Cl$_2$: δ_C = 53.84 ppm; residual CHDCl$_2$ in CD$_2$Cl$_2$: δ_H = 5.32 ppm); ^{1}H and ^{13}C assignments were established using NOESY, HSQC, and HMBC experiments; numbering schemes as shown in the inserts. C, H, and N elemental analyses were carried out on a Euro EA 3028HT CHNS/O analyzer (Pavia, Italy). Mass-spectra were obtained on a Bruker micrOTOF spectrometer equipped with the electrospray ionization (ESI) source (Bremen, Germany); MeOH, CH$_2$Cl$_2$, or MeOH/CH$_2$Cl$_2$ mixture was used as a solvent. Solvents were purified by distillation over the indicated drying agents and were transferred under Ar: Et$_2$O (Mg/anthracene), CH$_2$Cl$_2$ (CaH$_2$), hexane (Na/K). Flash chromatography: Merck Geduran® Si 60 (40–63 μm). Absorption spectra were measured in a 3.8 mL quartz cuvette using a UV-VIS spectrometer (UV-3600, Shimadzu, Kyoto, Japan) and photoluminescence emission and excitation spectra in the same cuvette, using a spectrofluorometer (RF-5031PC, Shimadzu). The luminescence quantum yield was determined using the slope method relative to the reference fluorophore, which the ethanol solution of Nile Blue dye (Φ = 0.27) excited at 590–625 nm, using a series of ethanol solutions of the sample with varying concentrations.

Synthesis of **9**. Methanol solution of NaOMe (30 wt %, 1.9 mmol, 356 μL) and a solution of *p*-diethylaminophenyldiazonium tetrafluoroborate (1.9 mmol, 500.0 mg) in 2 mL MeCN were sequentially added to a solution of diphenylimidazole 1 (1.9 mmol, 418.7 mg) in EtOH (10 mL). The resulting mixture was stirred for 1 h, evaporated, redissolved in CH$_2$Cl$_2$, filtered, evaporated again, washed with Et$_2$O (3 × 3 mL), and dried under vacuum. Yield: 674.2 mg (90%) Elem. anal. calcd. for C$_{25}$H$_{25}$N$_5$: C, 75.92; H, 6.37; N, 17.71. Found: C 76.13; H 6.54; N 17.58. ^{1}H NMR (400 MHz, CDCl$_3$): δ 9.74 (s, br, 1H), 7.90 (d, *J* = 9.1 Hz, 2H), 7.64 (m, 4 H), 7.38–7.31 (m, 6 H), 6.71 (d, *J* = 9.1 Hz, 2H), 3.47 (q, *J* = 7.0 Hz, 4H), 1.24 (t, *J* = 7.0 Hz, 6H). ^{13}C{^{1}H} NMR (151 MHz, CDCl$_3$): δ 211.8, 154.6, 150.9, 142.8, 135.5, 128.7, 128.5, 128.0, 126.2, 111.3, 44.9, 12.8. UV/Vis (CH$_2$Cl$_2$): λ_max = 493 nm, ε = 3.83 × 10^4 M^{-1} cm^{-1}.

Synthesis of **10**. Methanol solution (2 mL) of potassium *tert*-butoxide (189.4 mg, 1.69 mmol) and a solution of *p*-nitrophenyldiazonium tetrafluoroborate (1.69 mmol, 401.7 mg) in MeCN (10 mL) were sequentially added to a solution of di-*p*-methoxyphenylimidazole (1.69 mmol, 473.3 mg) in MeOH (20 mL). The resulting mixture was stirred for 1 h, evaporated, redissolved in CH$_2$Cl$_2$, filtered, evaporated again, washed with Et$_2$O (3 × 3 mL), and dried under vacuum. Yield: 374.1 mg (52%) Elem. anal. calcd. for C$_{23}$H$_{19}$N$_5$O$_4$: C, 64.33; H, 4.46; N, 16.31. Found: C 64.58; H 4.69; N 16.22. ^{1}H NMR (400 MHz, CDCl$_3$): δ 10.05 (s, br, 1H), 8.35 (d, *J* = 9.0 Hz, 2H), 8.01 (d, *J* = 9.0 Hz, 2H), 7.59 (m, 4H), 6.93 (d, *J* = 8.0 Hz, 4H), 3.85 (s, 6H). ^{13}C{^{1}H} NMR (151 MHz, CDCl$_3$): δ 160.1, 159.4, 155.5, 153.9, 148.2, 129.7, 129.3, 124.9, 123.0, 114.3, 55.4. UV/Vis (CH$_2$Cl$_2$): λ_max = 512 nm, ε = 1.92 × 10^4 M^{-1} cm^{-1}.

Synthesis of **11**. Methanol solution (2 mL) of potassium *t*-butoxide (165.6 mg, 1.49 mmol) and a solution of *p*-bromophenyldiazonium tetrafluoroborate (1.49 mmol, 403.5 mg) in MeCN (10 mL) were sequentially added to a solution of di-*p*-methoxyphenylimidazole (1.49 mmol, 413.5 mg) in MeOH (20 mL). The resulting mixture stirred for 1 h, evaporated, redissolved in CH$_2$Cl$_2$, filtered, evaporated again, washed with Et$_2$O (3 × 3 mL), and dried under vacuum. Yield: 374.1 mg (62%). Elem. anal. calcd. for C$_{23}$H$_{19}$N$_5$O$_4$: C 49.14; H 3.37; N 10.42. Found: C 49.56; H 3.74; N 10.11. ^{1}H NMR (400 MHz, CDCl$_3$): δ 9.86 (s, br, 1H), 7.82 (d, *J* = 8.8 Hz, 2H), 7.63 (d, *J* = 8.8 Hz, 4H), 7.46 (m, 2H), 6.91 (m, 4H), 3.84 (s, 6H). ^{13}C{^{1}H} NMR (151 MHz, CD$_3$CN): δ 159.5, 158.3, 154.0, 143.0, 132.8, 130.2, 130.0, 124.3, 114.5, 55.9. UV/Vis (CH$_2$Cl$_2$): λ_max = 483 nm, ε = 1.86 × 10^4 M^{-1} cm^{-1}.

General procedure for the synthesis of **7Zn–11Zn**, **7Cd–11Cd**, and **7Hg–11Hg**. Methanol solution of the ligand 9–11 (2 mL) was added to a solution of an appropriate metal halide (1 eq.) in 1 mL MeOH. The resulting mixture was kept without stirring for 24 h, the formed

precipitate was filtered, washed with MeOH (3 × 1 mL), Et$_2$O (3 × 3 mL), and dried under vacuum.

9Zn. 9 (1 eq, 0.13 mmol, 50.4 mg), ZnCl$_2$ (1 eq., 0.13 mmol, 17.8 mg) were used. Yield: 32.6 mg (48.2%). ^{1}H and ^{13}C NMR spectra were not obtained due to the low solubility of the compound in the common deuterated solvents. Elem. anal. calcd. for C$_{25}$H$_{25}$Cl$_2$N$_5$Zn: C, 56.46; H, 4.74; N, 13.17. Found: C 56.75; H 7.86; N 13.05. Crystals, suitable for X-ray analysis, were obtained from the reaction mixture. UV/Vis (CH$_2$Cl$_2$): λ_{max} = 614 nm, ε = 3.19 × 10^4 M^{-1} cm^{-1}.

9Cd. 9 (1 eq, 0.13 mmol, 50.2 mg), CdBr$_2$ 4H$_2$O (1 eq., 0.13 mmol, 44.0 mg) were used. Yield: 46.4 mg (54.9%). ^{1}H and ^{13}C NMR spectra were not obtained due to the low solubility of the compound in the common deuterated solvents. Elem. anal. calcd. for C$_{25}$H$_{25}$Br$_2$N$_5$Cd: C, 44.97; H, 3.77; N, 10.49. Found: C 45.14; H 3.98; N 10.38. UV/Vis (CH$_2$Cl$_2$): λ_{max} = 599 nm, ε = 3.03 × 10^4 M^{-1} cm^{-1}.

9Hg. 9 (1 eq, 0.13 mmol, 50.0 mg), HgCl$_2$ (1 eq., 0.13 mmol, 35.1 mg) were used. Yield: 46.0 mg (54.5%). ^{1}H and ^{13}C NMR spectra were not obtained due to the low solubility of the compound in the common deuterated solvents. Elem. anal. calcd. for C$_{25}$H$_{25}$Cl$_2$N$_5$Hg: C, 45.02; H, 3.78; N, 10.50. Found: C 45.31; H 3.87; N 10.46. Crystals, suitable for X-ray analysis, were obtained from the reaction mixture. UV/Vis (CH$_2$Cl$_2$): λ_{max} = 517 nm, ε = 3.13 × 10^4 M^{-1} cm^{-1}.

10Zn. 10 (2 eq., 0.17 mmol, 75.0 mg), ZnCl$_2$ (1 eq., 0.09 mmol, 12.2 mg) were used. Yield: 48.4 mg (55.5%). ^{1}H and ^{13}C NMR spectra were not obtained due to the low solubility of the compound in the common deuterated solvents. Elem. anal. calcd. for C$_{23}$H$_{19}$Cl$_2$N$_5$O$_4$Zn: C, 48.83; H, 3.39; N, 12.38. Found: C 49.11; H 3.56; N 12.29. UV/Vis (CH$_2$Cl$_2$): λ_{max} = 516 nm, ε = 7.70 × 10^4 M^{-1} cm^{-1}.

10Cd. 10 (2 eq., 0.17 mmol, 74.9 mg), CdBr$_2$ 4H$_2$O (1 eq., 0.09 mmol, 30.6 mg) were used. Yield: 66.6 mg (67.2%). ^{1}H and ^{13}C NMR spectra were not obtained due to the low solubility of the compound in the common deuterated solvents. Elem. anal. calcd. for C$_{23}$H$_{19}$Br$_2$N$_5$O$_4$Cd: C, 39.37; H, 2.73; N, 9.98. Found: C 39.71; H 2.94; N 10.05. Crystals, suitable for X-ray analysis, were obtained from the reaction mixture. UV/Vis (CH$_2$Cl$_2$): λ_{max} = 516 nm, ε = 6.67 × 10^4 M^{-1} cm^{-1}.

10Hg. 7 (2 eq., 0.17 mmol, 74.9 mg), HgCl$_2$ (1 eq., 0.09 mmol, 23.4 mg) were used. Yield: 45.0 mg (45.8%). ^{1}H and ^{13}C NMR spectra were not obtained due to the low solubility of the compound in the common deuterated solvents. Elem. anal. calcd. for C$_{23}$H$_{19}$Cl$_2$N$_5$O$_4$Hg: C, 39.41; H, 2.73; N, 9.99. Found: C 39.45; H 2.78; N 10.07. UV/Vis (CH$_2$Cl$_2$): λ_{max} = 517 nm, ε = 6.31 × 10^4 M^{-1} cm^{-1}.

11Zn. 11 (1 eq., 0.18 mmol, 50.3 mg), ZnCl$_2$ (1 eq., 0.18 mmol, 14.9 mg) were used. Yield: 26.3 mg (40.5%). ^{1}H and ^{13}C NMR spectra were not obtained due to the low solubility of the compound in the common deuterated solvents. Elem. anal. calcd. for C$_{23}$H$_{19}$BrCl$_2$ZnN$_4$O$_2$: C, 46.07; H, 3.19; N, 9.34. Found: C 45.87; H 3.08; N 9.36. UV/Vis (CH$_2$Cl$_2$): λ_{max} = 527 nm, ε = 2.14 × 10^4 M^{-1} cm^{-1}.

11Cd. 11 (1 eq., 0.11 mmol, 50.2 mg), CdBr$_2$·4H$_2$O (1 eq., 0.11 mmol, 37.2 mg) were used. Yield: 31.4 mg (39.7%). ^{1}H and ^{13}C NMR spectra were not obtained due to the low solubility of the compound in the common deuterated solvents. Elem. anal. calcd. for C$_{23}$H$_{19}$Br$_3$CdN$_4$O$_2$: C, 37.56; H, 2.60; N, 7.62. Found: C 37.64; H 2.66; N 7.81. UV/Vis (CH$_2$Cl$_2$): λ_{max} = 483 nm, ε = 1.03 × 10^4 M^{-1} cm^{1}.

11Hg. 11 (1 eq., 0.11 mmol, 50.0. mg), HgCl$_2$ (1 eq., 0.11 mmol, 29.9 mg) were used. Yield: 33.2 mg (41.62%). ^{1}H and ^{13}C NMR spectra were not obtained due to the low solubility of the compound in the common deuterated solvents. Elem. anal. calcd. for C$_{23}$H$_{19}$BrCl$_2$HgN$_4$O$_2$: C, 37.59; H, 2.61; N, 7.62. Found: C 37.81; H 2.54; N 7.58. UV/Vis (CH$_2$Cl$_2$): λ_{max} = 503 nm, ε = 2.24 × 10^4 M^{-1} cm^{1}.

2.1. X-ray Diffraction Studies

XRD data for **9Hg′**·2CH$_3$OH, **8**·solvate and **10Cd**·1.75CH$_3$OH·0.75H$_2$O were collected using equipment of the Center for Molecular Studies of the Nesmeyanov Institute of

Organoelement Compounds, Russian Academy of Sciences. The X-ray diffraction studies for **9Zn**·CH₃OH, **9Hg**·CH₃OH and **10** were performed at the Shared Equipment Center of the Kurnakov Institute of General and Inorganic Chemistry, Russian Academy of Sciences. The X-ray measurements were performed using shared experimental facilities supported by INEOS RAS and IGIC RAS state assignment.

Single crystals of **9Zn**·CH₃OH, **9Hg**·CH₃OH, **9Hg′**·2CH₃OH, **8**·solvate, **10** and **10Cd**· 1.75CH₃OH·0.75H₂O were obtained from reaction mixtures. Intensities of the reflections for these crystals were collected with Bruker D8 Venture (**9Zn**·CH₃OH, **9Hg**·CH₃OH, 10) and Bruker Quest (**9Hg**·2CH₃OH, **8**·solvate and **10Cd**·1.75CH₃OH·0.75H₂O) diffractometers (Bruker AXS, Inc., Madison, WI, USA) at 100.0(2) K (MoKα-radiation, λ = 0.71073 Å). The structures were solved by the SHELXT method [13] and refined by full-matrix least squares against F^2. Non-hydrogen atoms were refined anisotropically. H(N) and H(O) atoms were located on difference Fourier maps, and those of H(C) atoms were calculated. The unit cell of **8**·solvate contains two solvent molecules (each occupies 186 Å³ and has 50 counts of electrons), which were treated as a diffuse contribution to the overall scattering without specific atom positions by the SQUEEZE/PLATON procedure [14]. A similar procedure was applied to treat some of the highly disordered solvent molecules in **10Cd**; two voids with volumes 624 and 199 Å³ and 399 and 106 counts of electrons were found. All hydrogen atoms were included in a refinement by the riding model with U_{iso}(H) = 1.5U_{eq}(X) for methyl and hydroxy groups and 1.2U_{eq}(X) for the other atoms. All calculations were made using the SHELXL2014 [15] and OLEX2 [16] program packages. Crystallographic parameters and refinement details for all complexes are listed in Table S1. CCDC 2166661–2166666 contain the supplementary crystallographic data for this paper. These data can be obtained free of charge via http://www.ccdc.cam.ac.uk/structures/ (accessed on 10 April 2022).
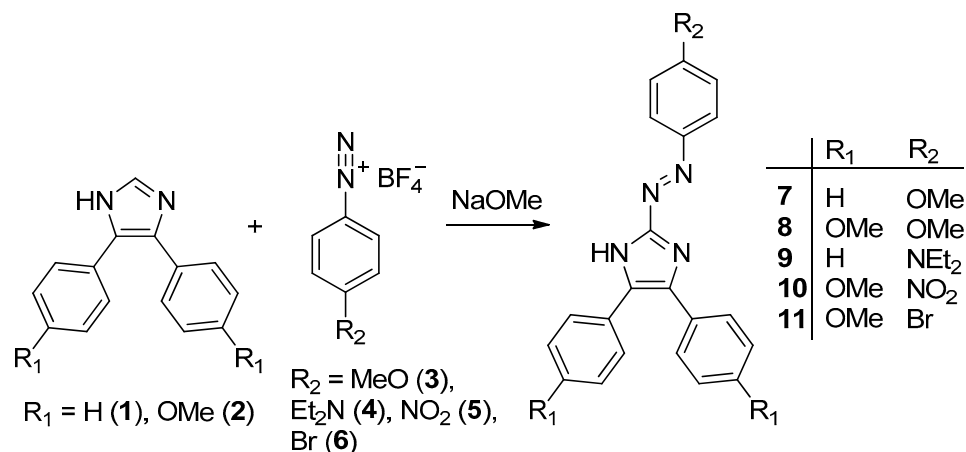
2.2. Computational Details

The DFT calculations based on the experimental X-ray geometries of **9Hg**, **9Hg′**, **9Zn**, and **10Cd** were carried out with the help of the Gaussian-09 [17] program package. The topological analysis of the electron density distribution was performed by using the Multiwfn program (version 3.7) [18]. The Cartesian atomic coordinates for model supramolecular associates are presented in the attached xyz-files, Supplementary Materials.

3. Results and Discussion

3.1. Synthesis and Structural Characterization

Novel triarylazoimidazoles **9–11** were readily synthesized by the coupling between the corresponding diazonium salts **4–6** and diarylimidazoles **1** or **2** (Scheme 1). The synthesis of similar triarylazoimidazoles **7** and **8** we reported earlier [2,12].

	R₁	R₂
7	H	OMe
8	OMe	OMe
9	H	NEt₂
10	OMe	NO₂
11	OMe	Br

R₁ = H (**1**), OMe (**2**)

R₂ = MeO (**3**), Et₂N (**4**), NO₂ (**5**), Br (**6**)

Scheme 1. Synthesis of triarylazoimidazoles **7–11**.

Triarylazoimidazoles **7–11** appear as bright red solids, **7**, **8**, **10**, and **11** [11] could be recrystallized from saturated MeOH solutions to produce crystals, suitable for analysis by single crystal X-ray crystallography (Figure 1). In addition, we obtained single crystals of **8** (Figure 1), which synthesis we reported earlier [2,12].
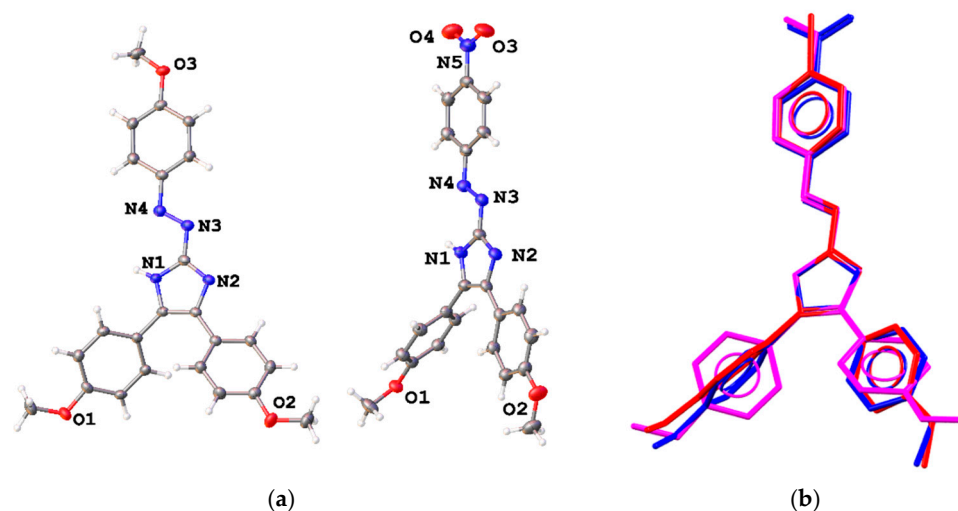

(**a**)   (**b**)

Figure 1. (**a**) Molecular structures of **8** and **10** in representation of atoms with thermal ellipsoids (given at p = 50%) and (**b**) comparison of their conformations with that of **11**. Solvent molecules are omitted. Overlaid atoms of **8** (magenta), **10** (blue), and **11** (red) belong to the imidazole ring.

Data about molecular and crystal structures of pure triarylazoimidazoles are limited with those for 2-(*p*-bromophenyl)diazen-1-yl-containing imidazole **11** [11]. Herein we compare its geometry with that of *p*-methoxy- and *p*-nitrosubstituted analogs. The main geometrical parameters of these molecules are listed in Table 1. Bond distances are very close for these molecules (Figure 1, Table 1). All molecules adopt a *trans* conformation with respect to the double N3=N4 bond. The azo double bond is elongated as compared with that in azobenzene, and the imidazole ring is nearly coplanar with the aryl group attached to the azo group (Figure 1). This fact indicates a prominent electron delocalization within the molecule. The two other substituents at carbon atoms of the five-membered ring can freely rotate along single C–C bonds, visualized in Figure 1.

Table 1. Selected geometrical parameters (Å, °) for azoimidazoles **7–11** and their group 12 metal complexes.

	9Zn	9Hg	9Hg′	8	10	10Cd	11
M-Hal	2.212(2)–2.221(1)	2.3905(9)–2.4210(8)	2.382(2)	-	-	2.595(1)–2.640(1)	-
M–N1$_{Pz}$	2.035(2)	2.280(2)	2.156(7)–2.220(6)	-	-	2.305(5)–2.392(5)	-
M–N4	2.137(2)	2.430(2)	2.430(8)	-	-	2.556(5)–2.885(6)	-
N–M–N	79.00(7)	70.08(8)	69.8(2)	-	-	62.2(2)–65.8(2)	-
Hal–M–Hal	115.15(5)	121.99(3)	-	-	-	103.8(3)–111.5(4)	-
N1–C3	1.386(2)	1.380(3)	1.358(10)	1.3868(1)	1.35887(6)	1.348(7)–1.384(8)	1.372(3)
N1=C1	1.346(2)	1.347(3)	1.321(10)	1.3595(1)	1.35986(8)	1.335(8)–1.373(8)	1.360(4)
C1–N2	1.337(2)	1.384(3)	1.338(10)	1.3253(1)	1.32652(7)	1.321(8)–1.352(8)	1.326(3)
C1–N3	1.378(3)	1.381(3)	1.354(10)	1.3904(1)	1.38415(7)	1.352(9)–1.389(8)	1.392(4)
N2–C2	1.387(2)	1.332(3)	1.356(10)	1.3806(1)	1.37085(8)	1.350(8)–1.395(8)	1.375(4)
C2=C3	1.392(3)	1.395(3)	1.385(11)	1.3962(1)	1.39362(7)	1.394(9)–1.421(9)	1.388(4)
N3=N4	1.296(2)	1.295(3)	1.252(9)	1.2742(1)	1.26990(7)	1.271(7)–1.299(8)	1.274(3)
Ar–C	1.470(3)–1.471(3)	1.472(3)–1.473(3)	1.454(10)–1.463(10)	1.4664(1)–1.4528(1)	1.46587(8)–1.48591(9)	1.443(8)–1.485(10)	1.474(3)–1.477(3)
ArvN4	1.380(2)	1.383(3)	1.386(10)	1.4224(1)	1.42510(7)	1.418(8)–1.437(8)	1.426(4)

Subsequent addition of group 12 metal chlorides to **7–11** resulted in the formation of chelates **7Zn–11Zn**, **7Cd–11Cd**, and **7Hg–11Hg** (Scheme 2), which precipitated from the reaction mixtures as dark purple microcrystalline solids. The crystals of complexes **9Zn**, **9Hg**, and **10Cd** were suitable for analysis by single crystal X-ray crystallography. The structural investigations proved the formation of azoimidazole chelate complexes

(Figure 2). The Cd complex **10Cd**, which contained *p*-NO$_2$ substituent by the azoaryl group, contained two chelating azoimidazoles in contrast to **9Zn** and **9Hg**.
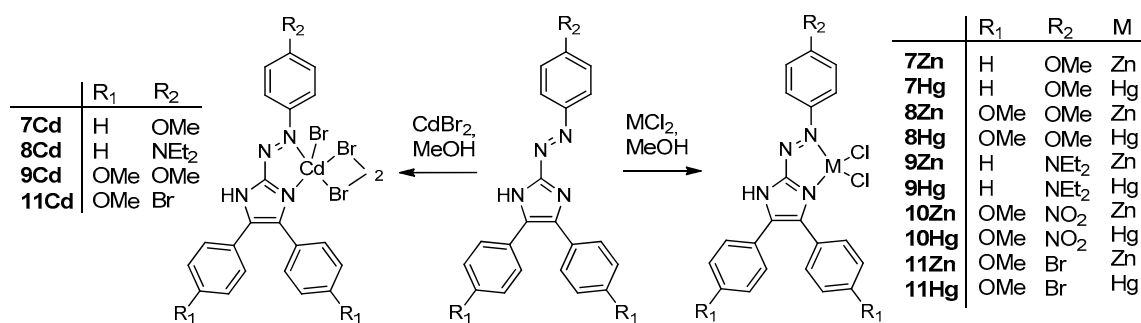
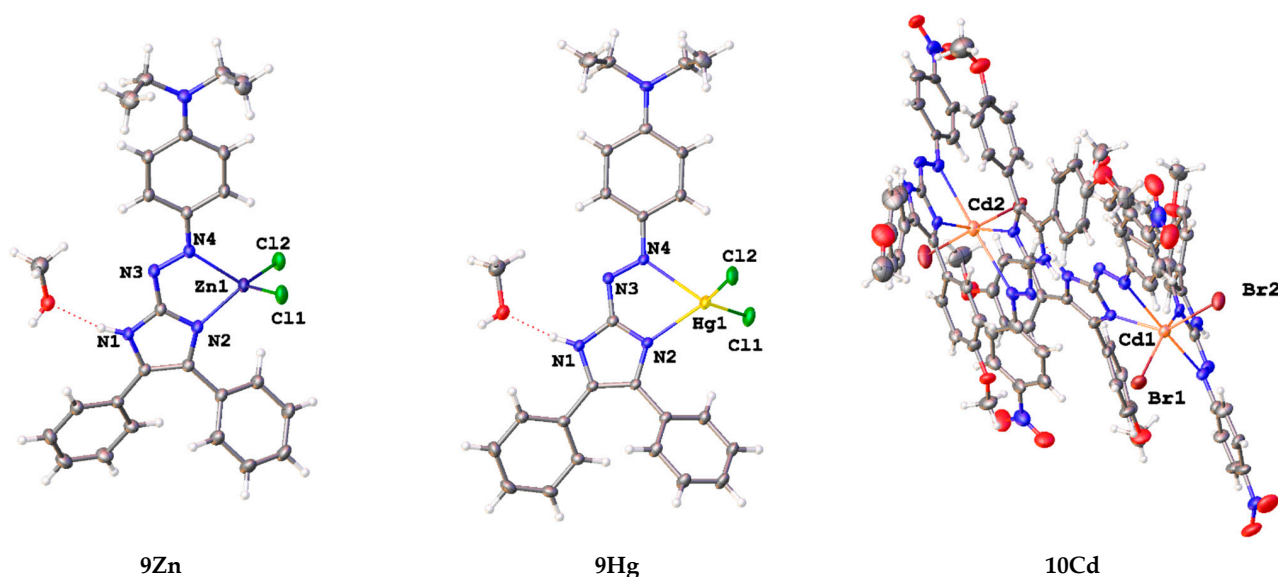**Scheme 2.** Synthesis of triarylazoimidazole complexes **7Zn–11Zn**, **7Cd–11Cd**, and **7Hg–11Hg**.

Figure 2. Asymmetric units of **9Zn**, **9Hg**, and **10Cd** in representation of atoms with thermal ellipsoids (given at p = 50%). Solvent molecules are omitted for **10Cd**.

Metal atoms in **9Zn** and **9Hg** complexes coordinate one azaimidazole ligand in a bidentate-chelate mode, and two terminal chlorine atoms to form a distorted tetrahedral MN$_2$Cl$_2$ coordination polyhedron. Asymmetric unit of **10Cd** contains two independent complexes. Their conformations are compared in Figure S2; they differ mainly in disposition of phenylmethoxy and nitrophenyl groups in respect to azoaimidazole fragments. In 10Cd, the large Cd^{2+} atom binds two chelating aza ligands and two terminal bromine atoms to form an octahedral CdN$_4$Br$_2$ coordination polyhedron with the nitrogen atoms of the azo group being in axial positions. Lengths of M–Cl, M–N1, and M–N4 bonds increase from Zn^{2+} to Hg^{2+} and to Cd^{2+} and N-M–N chelate angles decrease in the same raw (Table 1). Delocalization within the imidazole ring at coordination becomes less pronounced as it follows from elongation of single and shortening of double bonds; however, coordination of the azoaryl moiety results in elongation of the N=N bond and shortening of the N4–Ar and C1—N3 bonds. For all three complexes, all azoimidazoles retain upon coordination the *trans* configuration at diazo groups, and nearly planar configuration of the azoimidazole moieties. However, the N4 atom of the azo bond is situated on the same side as the N2 atom of the imidazole ring in respect to the C1–N3 bond, while for neutral ligands, it is always situated on the same side as the N1(H) atom of the ring. Interestingly, the N atom of the diethylamino group is also almost planar with CNC plane being coplanar with the

plane of the azoimidazole moiety, which indicates the significant electronic conjugation in the whole system.

Overall, molecular geometry of triarylazoimidazoles in **5**, **7–10** is similar to those reported for structurally relevant azo-compounds [5,9,19–25] and imidazole derivatives [26,27].

Interestingly, the reaction of **9** with $HgCl_2$ resulted in the formation of a very small batch of crystals of **9Hg′** (Figures 3 and S1) along with the main product **9Hg**. Although we were not able to reproduce the synthesis of **9Hg′**, here we give a description of the crystal structure of **9Hg′** since it is a remarkable one-dimensional coordination polymer. In this complex, chlorine atoms act as terminal ligands, and deprotonated azaimidazole **9** acts as a tridentate bridging and chelating ligand, which coordinates by both N atoms of the imidazole ring and the N4 atom of the azo group. Coordination bonds for the resulting tetrahedral HgN_2Cl_2 coordination polyhedron are very close to the **9Hg**, while delocalization within the five-membered ring becomes even more pronounced than in the neutral uncoordinated ligand (Table 1). Overall complex is a chain coordination polymer parallel with crystallographic axis c (Figure 3).
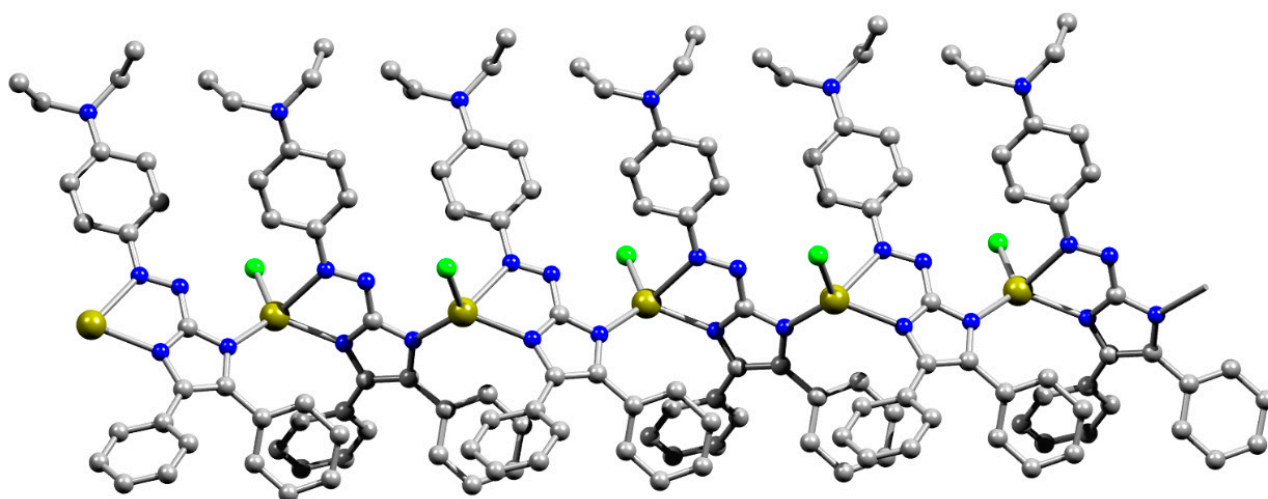

Figure 3. Ball-and-stick representation of the coordination polymer **9Hg′** in the crystal. Solvent molecules and hydrogen atoms are omitted. Color code: C–grey, Cl–green, H–light grey, Hg–olive green, N–blue, O–red.

Presence of acidic hydrogen atoms in **8**, **10**, **9Zn**, **9Hg**, and **10Cd** as well as a number of solvent water and MeOH molecules in solid **9Zn**, **9Hg**, **9Hg′**, and **10Cd** allows formation of strong H-bonds in these solids. Presence of some of these hydrogen bonds in metal complexes was confirmed using DFT calculations of isolate clusters followed by analysis of electron density distribution within the QTAIM approach (see Section 3.4) [28]. Herein we should note that in pure ligand **10** H-bonded dimers (see Figure S3) connected by two N-H . . . O bonds with a methoxy group were found (r(N . . . O) = 2.921(3)Å, NHO = 165.7°), while in **8**, one can propose that H(N) atom should be involved in H-bonding with acceptor groups of solvent molecules removed from refinement using the SQUEEZE procedure. In isostructural 9Zn and 9Hg H-bonded dimers (Figure S3) can be found due to N-H . . . O and O-H . . . Cl interactions with a hydroxy group of solvent molecule (r(N . . . O) = 2.747(3)–2.750(3)Å, NHO = 165.6–167.5°; r(O . . . Cl) = 3.104(3)–3.129(3) Å, OHCl = 163.1–165.0°). In 9Hg′, the amino group is absent, but methanol molecules are connected to the coordination polymer through O-H . . . O and O-H . . . Cl interactions (Figure S3; r(O . . . O) = 2.716(16) Å, OHO = 130.3°; r(O . . . Cl) = 3.124(10) Å, OHCl = 162.6°). In **10Cd**, one of the amino groups interacts with a bromine atom of a neighboring complex, two others with methanol molecules, and the fourth one with a water molecule. Solvent molecules in 10Cd also take part in O-H . . . O and O-H . . . Br bonding. Besides a strong hydrogen bond, C-H . . . Hal and C-H . . . O interactions can be found in solid **9Zn**, **9Hg**,

9Hg′, and **10Cd**. Planar configuration of the ligand also allows realization of hydrophobic C–H . . . π and stacking interactions in these compounds. Particularly, in H-bonded dimers in **9Zn** and **9Hg** the mean plains of ligands are situated parallel at distances 3.298(3) and 3.308(2) Å, respectively. Thus, geometry of these complexes allows realization of both hydrophilic and hydrophobic interactions in solids and ligand–receptor complexes.

3.2. Absorption and Emission Profiles

Ligands **7**–**10** exhibited a red color in the dichloromethane solution and the main absorption band with the absorption maximum close to 500 nm and additional absorption bands in the UV range (Figure 4, Table 2).
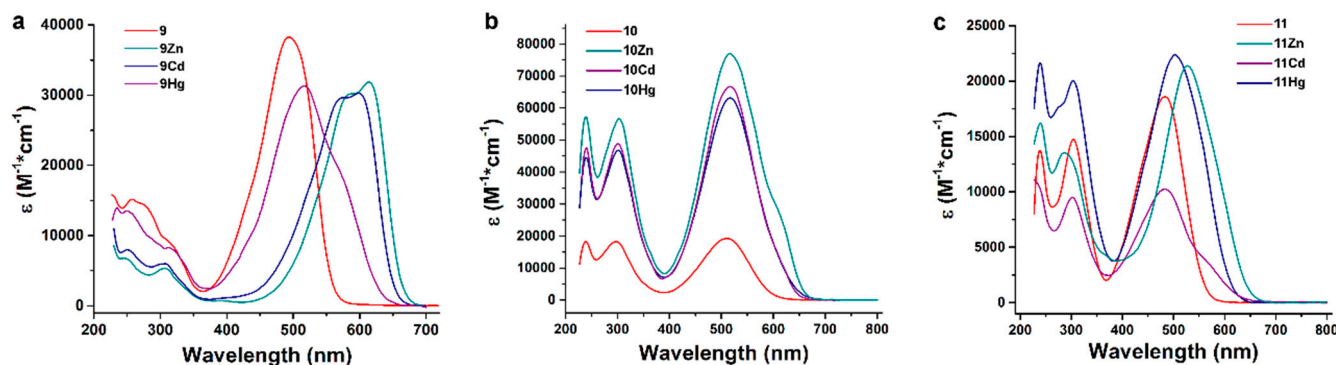

Figure 4. UV-Vis absorptions spectra of the ligand **9** and its complexes (**a**), ligand **10** and its complexes (**b**), ligand **11** and its complexes (**c**) in dichloromethane.

Table 2. UV-Vis absorption characteristics of the ligands **9**–**11** in dichloromethane solution.

	Absorption Maximum, nm	ε_{max}, M^{-1} cm^{-1}
9	493	38,300
10	512	19,200
11	483	18,600

Arylazoimidazole compounds have the absorption maximum in the near UV range around 360 nm corresponding to intraligand π–π* charge transfer (ILCT) transitions [29,30], the bathochromic shift of this maximum to 480–510 nm in ligands **9**–**11** can be partly attributed to electron delocalization effect due to the presence of two additional aromatic rings. Position and intensity of the ILCT absorption band is also affected by electron-donating and electron-withdrawing groups at the para-position of the aryl rings. In ligands **7** and **9**, the electron density shifts upon photoexcitation from the electron-donating OMe (Et$_2$N) group to the imidazole ring (electron acceptor). Correspondingly, in agreement with the previous findings [31] a stronger electron donor in the R$_1$ position gives **9** a higher absorption maximum (493 vs. 441 nm) and a larger extinction coefficient (38,300 vs. 28,300 M^{-1} cm^{-1}) compared to **7** [2]. Planar geometry of the arylazoimidazole fragment facilitates ILCT, thus producing large values of the extinction coefficients of **7** and **9**. In **8** and **10**–**11**, electron-donating methoxy groups at the R$_2$ position induce additional charge transfer from the aryl groups attached to the imidazole ring. This effect is further strengthened by the electron-withdrawing Br and NO$_2$ groups at the R$_1$ position, resulting in increase of absorption maximum from 466 (**8**) to 483 (**11**) and 512 nm (**10**). Lack of planarity between imidazole-attached aryl rings and imidazole hinders intraligand charge transfer and results in smaller values of extinction coefficients of the **8**, **10**, and **11** ligands compared with **7** and **9**. Extinction coefficients of **9**–**11** ligands corresponded to 22–28,000 M^{-1} cm^{-1} values reported for similar arylazoimidazole and triarylazoimidazole compounds [2].

The ILCT absorption bands of the ligands **9** and **11** exhibited a bathochromic shift, which was especially strong in case of Zn and Cd complexes of **9** giving them inten-

sive blue colors (Figure 4, Table 2). The same coordination-induced spectral shift was previously discovered for the complexes of **7** and **8** [2]. This shift is attributed to the electron-withdrawing effect of metal ions coordinated to the azo group and imidazole ring and depends on the LUMO at the N1 and N4 nitrogen atoms. Thus, the strongest coordination-induced absorption shift was observed for complexes of **9** (from 493 to ca. 590 nm in **9Zn**), where electron density in the excited state was localized at the imidazole ring as a result of charge transfer induced by the Et_2N substituent. At the same time, in ligand **10**, the nitro group itself exerted a strong electron-withdrawing effect via the aromatic ring and attracted electron density from the azo and imidazole groups; as a result the bathochromic shift of the absorption maximum induced by coordination was small (from 512 to 516 nm). The complexes of **11** with a weakly electron-withdrawing Br atom at the R_1 position exhibited an intermediate shift (from 483 to 527 nm). Coordination-induced bathochromic shift of the ILCT band also depended on the metal ion and followed the trend $\lambda_{maxILCT}(Hg) < \lambda_{maxILCT}(Cd) < \lambda_{maxILCT}(Zn)$ [2]. Additional absorption bands appeared in the UV-Vis spectra of complexes in the spectral region between 580 and 620 nm and is attributed to metal-to-ligand charge transfer (MLCT) transition. In case of complexes **9Zn** and **9Cd**, this coordination-induced MLCT band was even stronger than the ILCT band at 550–560 nm, for others it appeared as a shoulder on the absorption spectrum.

Whereas ligands **9**–**11** were nonluminescent, all complexes exhibited red photoluminescence emission in dichloromethane solutions with emission maximum between 650 and 680 nm (Figure 4, Table 3), similar orange or red photoluminescence with emission maximum between 600 and 660 nm was previously observed for the metal complexes of **7** and **8** [2].

Table 3. UV-Vis absorption and photoluminescence characteristics of the complexes **9Zn**–**11Zn**, **9Cd**–**11Cd**, and **9Hg**–**11Hg** in dichloromethane solution.

	Absorption Maximum, nm	ε_{max}, $M^{-1}\ cm^{-1}$	Excitation Maximum, nm	Emission Maximum, nm	PL Quantum Yield, %
9Zn	614	31,900	626	662	1.13
9Cd	599	30,300	613	653	0.60
9Hg	517	31,300	596	650	0.2
10Zn	516	77,000	621	661	16.7
10Cd	516	66,700	614	662	4.7
10Hg	517	63,100	609	661	2.6
11Zn	527	21,400	590	677	21.0
11Cd	483	10,250	580	668	18.8
11Hg	503	22,400	549	657	0.01

Excitation and emission maximum wavelengths followed the general trend $\lambda_{ex(em)}$ (Hg) < $\lambda_{ex(em)}$ (Cd) < $\lambda_{ex(em)}$ (Zn), and the luminescence quantum yields–Φ (Hg) < Φ (Cd) < Φ (Zn) in accordance with the trend found for metal complexes of **7** and **8** [2]. Luminescence excitation maxima coincided with the positions of MLCT absorption bands on UV-Vis spectra of complexes, which confirms that emission is excited via coordination-related MLCT transitions. R_1 and R_2 substituents in **9**–**11** strongly affected the luminescence quantum yield (Table 3). The maximal quantum yield (21% for **11Zn**) is smaller than the yield of **7** and **8** metal complexes (up to 44%) [2] but was still significant.

3.3. Antibacterial Tests

The in vitro antibacterial activity of the **7**–**11** against Gram-positive microorganism *S. aureus* and Gram-negative microorganism *E. coli* was estimated using the agar-well diffusion method. The antibacterial properties of **7**–**11** (Table 4) were compared with those for the commercially available conventional antibiotics ampicillin and gentamicin. The antibacterial activities of the mentioned organic compounds increase in the row **7** < **8**~**10** < **11** < **9**, where **9** is the undoubted leader (see the corresponding inhibition zones and, especially, MIC values). We assume that the antibacterial pharmacophore is an azaimidazole moiety,

which can be highly protonated at physiological pH. The resulting cation interacts with the anionic fragments of bacterial cell surface, which causes an osmotic imbalance, damages of the bacterial cell membrane, and leakage of the cell content into the external environment. The cascade of these unfavorable events for the bacterial cell inevitably leads to the death of the bacterium. The intracellular components of bacteria are characterized by strong absorption at 260 nm. This fact was used in previous studies to monitor the integrity of the bacterial cell membrane by spectrophotometry. We used this approach within the frames of the current work to study the effect of **7–11** on the integrity of the cell membranes of *S. aureus* and *E. coli*. We found that treatment of the bacterial suspension with **7–11** caused a dramatic increase in optical density from 0.5 to 0.9 in 6 min (**9**), 10 min (**8, 10, 11**), or 20 min (**7**). Thus, the tested organic compounds effectively damaged the bacterial cell membrane, but the effect of **9** most rapidly developed. The highest antibacterial effect of **9** can be explained by the presence of a larger number of N-atoms that can be protonated at a physiological pH value.

Table 4. The in-vitro antibacterial activity of the ligands **7–11** and their complexes against Gram-positive microorganism *S. aureus* and Gram-negative microorganism *E. coli*.

	S. aureus	*E. coli*
	Inhibition Zone, mm/MIC	
7	$20.4 \pm 0.1/1.11$	$18.3 \pm 0.2/1.13$
8	$22.3 \pm 0.2/0.97$	$19.1 \pm 0.3/0.99$
9	$23.6 \pm 0.1/0.81$	$20.1 \pm 0.3/0.79$
10	$22.1 \pm 0.3/0.97$	$19.1 \pm 0.2/0.99$
11	$22.6 \pm 0.1/0.95$	$19.1 \pm 0.2/0.95$
7Zn	$23.8 \pm 0.2/0.87$	$19.9 \pm 0.2/0.81$
7Cd	$25.2 \pm 0.1/0.63$	$18.9 \pm 0.3/0.75$
7Hg	$28.7 \pm 0.3/0.34$	$20.2 \pm 0.2/0.63$
8Zn	$24.5 \pm 0.3/0.77$	$19.7 \pm 0.1/0.83$
8Cd	$26.9 \pm 0.3/0.51$	$20.4 \pm 0.2/0.63$
8Hg	$30.1 \pm 0.2/0.19$	$21.0 \pm 0.2/0.51$
9Zn	$25.0 \pm 0.1/0.63$	$20.9 \pm 0.2/0.58$
9Cd	$28.5 \pm 0.2/0.32$	$21.8 \pm 0.3/0.43$
9Hg	$33.4 \pm 0.3/0.11$	$22.9 \pm 0.1/0.22$
10Zn	$24.8 \pm 0.1/0.74$	$19.8 \pm 0.4/0.82$
10Cd	$26.5 \pm 0.1/0.52$	$20.9 \pm 0.1/0.65$
10Hg	$30.4 \pm 0.2/0.18$	$21.0 \pm 0.3/0.50$
11Zn	$24.4 \pm 0.2/0.75$	$19.5 \pm 0.1/0.80$
11Cd	$27.3 \pm 0.3/0.49$	$20.6 \pm 0.1/0.62$
11Hg	$30.0 \pm 0.3/0.20$	$21.2 \pm 0.3/0.51$
Ampicillin	$30.2 \pm 0.2/0.12$	–
Gentamicin	–	$22.1 \pm 0.2/0.21$

The antibacterial activity of Zn(II), Cd(II), and Hg(II) complexes derived from **7–11** is substantially higher than that of the staring **7–11** (Table 1). Provided the same metal center, the complexes derived from **9** are characterized by the highest antibacterial effect, while the complexes derived from **7** are the least active. Moreover, provided the same ligand, the antibacterial activity of complexes increases in the rows Zn(II), Cd(II), Hg(II), and this corresponds to the previously reported data about antibacterial activity of Zn(II), Cd(II), and Hg(II) complexes with glibenclamide or 2,6-bis(benzimidazol-2-yl) pyridine ligands [32,33]. Thus, the most effective antibacterial complex proved to be **9Hg**. The antibacterial activity of this complex is almost equal to that of the reference antibiotics ampicillin and gentamicin.

3.4. Theoretical Studies of Intermolecular Hydrogen Bonding Interactions N–H···O, O–H···Cl, and N–H···Br in **9Hg**, **9Hg'**, **9Zn**, and **10Cd**

In order to confirm or disprove the hypothesis on the existence of various most interesting intermolecular hydrogen bonding interactions N–H···O, O–H···Cl, and N–H···Br in **9Hg**, **9Hg'**, **9Zn**, and **10Cd**, and approximately quantify the strength of these supramolecular contacts from a theoretical viewpoint, the DFT calculations followed by the topological analysis of the electron density distribution within the QTAIM approach [28] were carried out at the ωB97XD/SDD level of theory for model supramolecular associates (see computational details and attached xyz-files in Supplementary Materials). Results of QTAIM analysis summarized in Table 5, the contour line diagrams of the Laplacian of electron density distribution $\nabla^2\rho(r)$, bond paths, and selected zero-flux surfaces, visualization of electron localization function (ELF), and reduced density gradient (RDG) analyses for the selected intermolecular hydrogen bonding interactions N–H···O, O–H···Cl, and N–H···Br in **9Hg** and **10Cd** are shown in Figure 5 for illustrative purposes.

Table 5. Characteristics of H-bonds in **9Hg**, **9Hg'**, **9Zn**, and **10Cd** *.

Contact	r(A ... D)	AHD	$\rho(r)$	$\nabla^2\rho(r)$	λ_2	H_b	V(r)	G(r)	E_{int}
				9Hg					
N–H···O	2.747(3)	167.5	0.031	0.135	−0.031	0.002	−0.030	0.032	9.4
O–H···Cl[i]	3.129(3)	163.1	0.020	0.063	−0.020	0.000	−0.016	0.016	5.0
				9Hg'					
O–H···Cl	3.124(10)	162.6	0.020	0.064	−0.020	0.000	−0.016	0.016	5.0
				9Zn					
N–H···O	2.750(3)	165.6	0.030	0.124	−0.030	0.002	−0.028	0.030	8.8
N[i]–H[i]···O[i]	2.750(3)	165.6	0.031	0.129	−0.031	0.002	−0.029	0.031	9.1
O–H···Cl[i]	3.104(3)	165.0	0.022	0.068	−0.022	0.000	−0.017	0.017	5.3
O[i]–H[i]···Cl	3.104(3)	165.0	0.020	0.064	−0.020	0.000	−0.016	0.016	5.0
				10Cd					
N–H···Br	3.282(5)	173.7	0.020	0.061	−0.020	0.000	−0.015	0.015	4.7

* r(A ... D)—bond distance (Å); AHD—bond angle (°); $\rho(r)$—values of the density of all electrons, $\nabla^2\rho(r)$—Laplacian of electron density, λ_2—appropriate eigenvalues, H_b—energy density, V(r)—potential energy density, G(r)—Lagrangian kinetic energy (a.u.) at the bond critical points (3, −1), corresponding to intermolecular hydrogen bonding interactions and strength for these contacts E_{int} (kcal/mol) estimated as −V(r)/2 [34]. Symmetry codes to generate equivalent atoms in crystal structures: (i) 1–x, 1–y, 1–z.
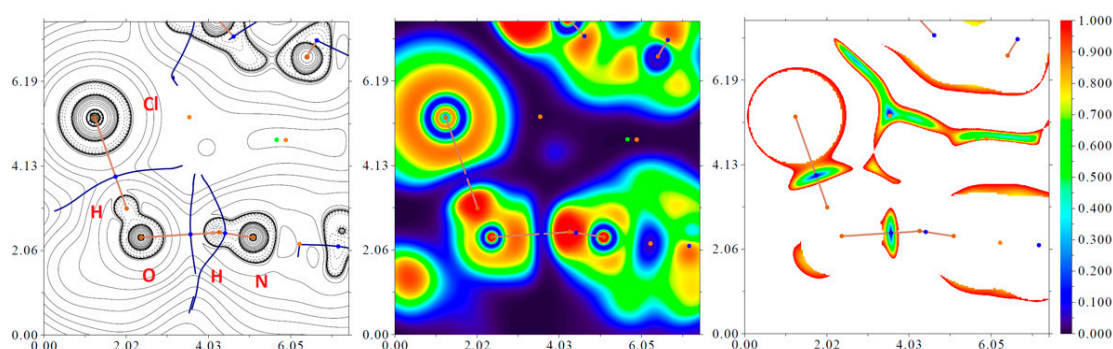

Figure 5. Contour line diagram of the Laplacian of electron density distribution $\nabla^2\rho(r)$, bond paths, and selected zero-flux surfaces (**left** panel), visualization of electron localization function (ELF, **center** panel), and reduced density gradient (RDG, **right** panel) analyses for intermolecular hydrogen bonding interactions N–H···O and O–H···Cl in **9Hg**. Bond critical points (3, −1) are shown in blue, nuclear critical points (3, −3)—in pale brown, ring critical points (3, +1)—in orange, cage critical points (3, +3)—in light green, bond paths are shown as pale brown lines, length units—Å, and the color scale for the ELF and RDG maps is presented in a.u.

The QTAIM analysis of model supramolecular associates demonstrates the presence of intermolecular hydrogen bonding interactions N–H···O, O–H···Cl, and N–H···Br in **9Hg**, **9Hg′**, **9Zn**, and **10Cd** (Table 5). The low magnitude of the electron density (0.020–0.031 a.u.), positive values of the Laplacian of electron density (0.061–0.135 a.u.), and zero or very close to zero positive energy density (0.000–0.002 a.u.) in these bond critical points (3, –1) as well as the estimated strength of appropriate supramolecular contacts (4.7–9.4 kcal/mol) are typical for hydrogen bonds in such chemical systems [23,35–37]. The balance between the Lagrangian kinetic energy G(r) and potential energy density V(r) at the bond critical points (3, –1) reveals that a covalent contribution in all discussed intermolecular hydrogen bonding interactions N–H···O, O–H···Cl, and N–H···Br in **9Hg**, **9Hg′**, **9Zn**, and **10Cd** is absent, and a sign of λ_2 indicates that these supramolecular contacts are attractive.

4. Conclusions

Overall, we reported the synthesis and characterization of novel triarylazoimidazoles and their group 12 metal complexes. Two triarylazoimidazoles (8 and 10) and four of their metal complexes (**9Zn**, **9Hg**, **9Hg**, **10Cd**) were structurally characterized. Novel complexes exhibit red photoluminescence emission (Φ up to 0.21) in a solution. Moreover, the antibacterial activity of complexes was tested against Gram-positive microorganism *S. aureus* and Gram-negative microorganism *E. coli*.

Author Contributions: Conceptualization, A.G.T.; methodology, A.S.K. (Andreii S. Kritchenkov); investigation, A.A.A. (Alexey A. Artemjev), A.A.A. (Artyom A. Astafiev), A.V.V. and A.S.K. (Alexey S. Kubasov); writing—original draft preparation, A.G.T. and G.M.B.; writing—review and editing, A.G.T., A.A.K. and A.S.N. All authors have read and agreed to the published version of the manuscript.

Conflicts of Interest: The authors declare no conflict of interest.

References

1. Otsuki, J.; Suwa, K.; Sarker, K.K.; Sinha, C. Photoisomerization and thermal isomerization of arylazoimidazoles. *J. Phys. Chem. A* **2007**, *111*, 1403–1409. [CrossRef] [PubMed]
2. Astafiev, A.A.; Repina, O.V.; Tupertsev, B.S.; Nazarov, A.A.; Gonchar, M.R.; Vologzhanina, A.V.; Nenajdenko, V.G.; Kritchenkov, A.S.; Khrustalev, V.N.; Nadtochenko, V.N.; et al. Unprecedented Coordination-Induced Bright Red Emission from Group 12 Metal-Bound Triarylazoimidazoles. *Molecules* **2021**, *26*, 1739. [CrossRef] [PubMed]
3. Crespi, S.; Simeth, N.A.; König, B. Heteroaryl azo dyes as molecular photoswitches. *Nat. Rev. Chem.* **2019**, *3*, 133–146. [CrossRef]
4. Sarker, K.K.; Chand, B.G.; Suwa, K.; Cheng, J.; Lu, T.H.; Otsuki, J.; Sinha, C. Structural studies and photochromism of mercury(II)-iodo complexes of (arylazo)imidazoles. *Inorg. Chem.* **2007**, *46*, 670–680. [CrossRef]
5. Liu, Y.; Varava, P.; Fabrizio, A.; Eymann, L.Y.M.; Tskhovrebov, A.G.; Planes, O.M.; Solari, E.; Fadaei-Tirani, F.; Scopelliti, R.; Sienkiewicz, A.; et al. Synthesis of aminyl biradicals by base-induced Csp3–Csp3 coupling of cationic azo dyes. *Chem. Sci.* **2019**, *10*, 5719–5724. [CrossRef]
6. Sarker, K.K.; Sardar, D.; Suwa, K.; Otsuki, J.; Sinha, C. Cadmium (II) complexes of (Arylazo)imidazoles: Synthesis, structure, photochromism, and density functional theory calculation. *Inorg. Chem.* **2007**, *46*, 8291–8301. [CrossRef]
7. Das, D.; Nayak, M.K.; Sinha, C. Chemistry of azoimidazoles. Synthesis, spectral characterization and redox studies of N(1)-benzyl-2-(arylazo)imidazolepalladium(II)chloride. *Transit. Met. Chem.* **1997**, *22*, 172–175. [CrossRef]

8. Schütt, C.; Heitmann, G.; Wendler, T.; Krahwinkel, B.; Herges, R. Design and synthesis of photodissociable ligands based on azoimidazoles for light-driven coordination-induced spin state switching in homogeneous solution. *J. Org. Chem.* **2016**, *81*, 1206–1215. [CrossRef]

9. Tskhovrebov, A.G.; Naested, L.C.E.; Solari, E.; Scopelliti, R.; Severin, K. Synthesis of azoimidazolium dyes with nitrous oxide. *Angew. Chem. Int. Ed.* **2015**, *54*, 1289–1292. [CrossRef]

10. Bhunia, P.; Baruri, B.; Ray, U.; Sinha, C.; Das, S.; Cheng, J.; Lu, T.-H. Azoimidazole Complexes of Manganese (II)-thiocyanate. X-ray Structures of 2-(p-tolylazo)imidazole and Bis-[1-methyl-2-(p-tolylazo)imidazole]-Di-thiocyanato-manganese(II). *Transit. Met. Chem.* **2006**, *31*, 310–315. [CrossRef]

11. Temesgen, A.; Tskhovrebov, A.G.; Vologzhanina, A.V.; Le, T.A.; Khrustalev, V.N. Crystal structure of 2-[(*E*)-2-(4-bromophenyl)diazen-1-yl]-4,5-bis(4-methoxyphenyl)-1*H*-imidazole: The first example of a structurally characterized triarylazoimidazole. *Acta Crystallogr. Sect. E* **2021**, *77*, 305–308. [CrossRef]

12. Tskhovrebov, A.G.; Novikov, A.S.; Tupertsev, B.S.; Nazarov, A.A.; Antonets, A.A.; Astafiev, A.A.; Kritchenkov, A.S.; Kubasov, A.S.; Nenajdenko, V.G.; Khrustalev, V.N. Azoimidazole Gold(III) Complexes: Synthesis, Structural Characterization and Self-Assembly in the Solid State. *Inorg. Chim. Acta* **2021**, *522*, 120373. [CrossRef]

13. Sheldrick, G.M. SHELXT—Integrated space-group and crystal-structure determination. *Acta Crystallogr. Sect. A Found. Crystallogr.* **2015**, *71*, 3–8. [CrossRef] [PubMed]

14. Spek, A.L. PLATON SQUEEZE: A tool for the calculation of the disordered solvent contribution to the calculated structure factors. *Acta Crystallogr. Sect. C* **2015**, *71*, 9–18. [CrossRef] [PubMed]

15. Sheldrick, G.M. Crystal structure refinement with SHELXL. *Acta Crystallogr. Sect. C Struct. Chem.* **2015**, *71*, 3–8. [CrossRef] [PubMed]

16. Dolomanov, O.V.; Bourhis, L.J.; Gildea, R.J.; Howard, J.A.K.; Puschmann, H. OLEX2: A complete structure solution, refinement and analysis program. *J. Appl. Crystallogr.* **2009**, *42*, 339–341. [CrossRef]

17. Frisch, M.J.; Trucks, G.W.; Schlegel, H.B.; Scuseria, G.E.; Robb, M.A.; Cheeseman, J.R.; Scalmani, G.; Barone, V.; Mennucci, B.; Petersson, G.A.; et al. *Gaussian 09 C.01*; Gaussian, Inc.: Wallingford, CT, USA, 2010.

18. Lu, T.; Chen, F. Multiwfn: A multifunctional wavefunction analyzer. *J. Comput. Chem.* **2012**, *33*, 580–592. [CrossRef]

19. Tskhovrebov, A.G.; Solari, E.; Scopelliti, R.; Severin, K. Reactions of grignard reagents with nitrous oxide. *Organometallics* **2014**, *33*, 2405–2408. [CrossRef]

20. Eymann, L.Y.M.; Tskhovrebov, A.G.; Sienkiewicz, A.; Bila, J.L.; Živković, I.; Rønnow, H.M.; Wodrich, M.D.; Vannay, L.; Corminboeuf, C.; Pattison, P.; et al. Neutral Aminyl Radicals Derived from Azoimidazolium Dyes. *J. Am. Chem. Soc.* **2016**, *138*, 15126–15129. [CrossRef]

21. Nenajdenko, V.G.; Shikhaliyev, N.G.; Maharramov, A.M.; Bagirova, K.N.; Suleymanova, G.T.; Novikov, A.S.; Khrustalev, V.N.; Tskhovrebov, A.G. Halogenated Diazabutadiene Dyes: Synthesis, Structures, Supramolecular Features, and Theoretical Studies. *Molecules* **2020**, *25*, 5013. [CrossRef]

22. Tskhovrebov, A.G.; Vasileva, A.A.; Goddard, R.; Riedel, T.; Dyson, P.J.; Mikhaylov, V.N.; Serebryanskaya, T.V.; Sorokoumov, V.N.; Haukka, M. Palladium(II)-Stabilized Pyridine-2-Diazotates: Synthesis, Structural Characterization, and Cytotoxicity Studies. *Inorg. Chem.* **2018**, *57*, 930–934. [CrossRef] [PubMed]

23. Repina, O.V.; Novikov, A.S.; Khoroshilova, O.V.; Kritchenkov, A.S.; Vasin, A.A.; Tskhovrebov, A.G. Lasagna-like supramolecular polymers derived from the PdII osazone complexes via C(sp2)–H···Hal hydrogen bonding. *Inorg. Chim. Acta* **2020**, *502*, 119378. [CrossRef]

24. Shikhaliyev, N.G.; Maharramov, A.M.; Bagirova, K.N.; Suleymanova, G.T.; Tsyrenova, B.D.; Nenajdenko, V.G.; Novikov, A.S.; Khrustalev, V.N.; Tskhovrebov, A.G. Supramolecular organic frameworks derived from bromoaryl-substituted dichlorodiazabutadienes via Cl·Br halogen bonding. *Mendeleev Commun.* **2021**, *31*, 191–193. [CrossRef]

25. Shikhaliyev, N.G.; Maharramov, A.M.; Suleymanova, G.T.; Babazade, A.A.; Nenajdenko, V.G.; Khrustalev, V.N.; Novikov, A.S.; Tskhovrebov, A.G. Arylhydrazones of α-keto esters via methanolysis of dichlorodiazabutadienes: Synthesis and structural study. *Mendeleev Commun.* **2021**, *31*, 677–679. [CrossRef]

26. Tskhovrebov, A.G.; Lingnau, J.B.; Fürstner, A. Gold Difluorocarbenoid Complexes: Spectroscopic and Chemical Profiling. *Angew. Chem. Int. Ed.* **2019**, *58*, 8834–8838. [CrossRef]

27. Tskhovrebov, A.G.; Goddard, R.; Fürstner, A. Two Amphoteric Silver Carbene Clusters. *Angew. Chem. Int. Ed.* **2018**, *57*, 8089–8094. [CrossRef]

28. Bader, R.F.W. A Quantum Theory of Molecular Structure and Its Applications. *Chem. Rev.* **1991**, *91*, 893–928. [CrossRef]

29. Ostrowska, K.; Stadnicka, K.M.; Gryl, M.; Klimas, O.; Brela, M.Z.; Goszczycki, P.; Liberka, M.; Grolik, J.; Węgrzyn, A. Influence of Hydrogen Bonds and π–π Interactions on the Fluorescence of Crystalline (*N*-Alkylpyridyl)enamino-pyrrolo [2,3-b]quinoxalin-2-one Derivatives. *Cryst. Growth Des.* **2022**, *22*, 1571–1582. [CrossRef]

30. Anitha, C.; Sheela, C.D.; Tharmaraj, P.; Shanmugakala, R. Studies on Synthesis and Spectral Characterization of Some Transition Metal Complexes of Azo-Azomethine Derivative of Diaminomaleonitrile. *Int. J. Inorg. Chem.* **2013**, *2013*, 436275. [CrossRef]

31. Pramanik, A.; Basu, A.; Das, G. Coordination assembly of p-substituted aryl azo imidazole complexes: Influences of electron donating substitution and counter ions. *Polyhedron* **2010**, *29*, 1980–1989. [CrossRef]

32. Aghatabay, N.M.; Neshat, A.; Karabiyik, T.; Somer, M.; Haciu, D.; Dülger, B. Synthesis, characterization and antimicrobial activity of Fe(II), Zn(II), Cd(II) and Hg(II) complexes with 2,6-bis(benzimidazol-2-yl) pyridine ligand. *Eur. J. Med. Chem.* **2007**, *42*, 205–213. [CrossRef] [PubMed]

33. Rasheed, K.; Tariq, M.I.; Munir, C.; Hussain, I.; Siddiqui, H.L. Synthesis, Characterization and Hypoglycemic Activity of Zn(II), Cd(II) and Hg(II) Complexes with Glibenclamide. *Chem. Pharm. Bull.* **2008**, *56*, 168–172. [CrossRef] [PubMed]

34. Espinosa, E.; Molins, E.; Lecomte, C. Hydrogen bond strengths revealed by topological analyses of experimentally observed electron densities. *Chem. Phys. Lett.* **1998**, *285*, 170–173. [CrossRef]

35. Serebryanskaya, T.V.; Novikov, A.S.; Gushchin, P.V.; Haukka, M.; Asfin, R.E.; Tolstoy, P.M.; Kukushkin, V.Y. Identification and H(D)-bond energies of C-H(D) Cl interactions in chloride-haloalkane clusters: A combined X-ray crystallographic, spectroscopic, and theoretical study. *Phys. Chem. Chem. Phys.* **2016**, *18*, 14104–14112. [CrossRef]

36. Tskhovrebov, A.G.; Novikov, A.S.; Odintsova, O.V.; Mikhaylov, V.N.; Sorokoumov, V.N.; Serebryanskaya, T.V.; Starova, G.L. Supramolecular polymers derived from the PtII and PdII schiff base complexes via C(sp2)–H . . . Hal hydrogen bonding: Combined experimental and theoretical study. *J. Organomet. Chem.* **2019**, *886*, 71–75. [CrossRef]

37. Mikhaylov, V.N.; Sorokoumov, V.N.; Novikov, A.S.; Melnik, M.V.; Tskhovrebov, A.G.; Balova, I.A. Intramolecular hydrogen bonding stabilizes trans-configuration in a mixed carbene/isocyanide PdII complexes. *J. Organomet. Chem.* **2020**, *912*, 121174. [CrossRef]